Short communication

Pt–SnO₂/nitrogen-doped CNT hybrid catalysts for proton-exchange membrane fuel cells (PEMFC): Effects of crystalline and amorphous SnO₂ by atomic layer deposition

Yougui Chen [a], Jiajun Wang [a], Xiangbo Meng [a], Yu Zhong [a], Ruying Li [a], Xueliang Sun [a,*], Siyu Ye [b], Shanna Knights [b]

[a] Department of Mechanical and Materials Engineering, University of Western Ontario, London, Ontario N6A 5B9, Canada
[b] Ballard Power Systems Inc., 9000 Glenlyon Parkway, Burnaby, BC V5J 5J8, Canada

HIGHLIGHTS

- Pt–SnO₂/nitrogen-doped carbon nanotubes hybrid catalyst.
- Enhanced electrochemical stability with the addition of SnO₂.
- Crystalline SnO₂ is more effective in stabilizing Pt catalysts than the amorphous one.
- Controllable deposition of crystalline and amorphous SnO₂ by atomic layer deposition.

ARTICLE INFO

ABSTRACT

SnO₂ and Pt nanoparticles were deposited on nitrogen-doped CNT (CNₓ) in sequence to construct a Pt–SnO₂/CNₓ hybrid electrocatalyst for proton-exchange membrane fuel cells (PEMFC). Crystalline and amorphous SnO₂ were deposited selectively by controlling the temperature via atomic layer deposition method. The electrochemical stability of Pt catalyst was enhanced with the addition of SnO₂, as demonstrated by accelerated durability tests. Furthermore, the crystalline SnO₂ was more effective than the amorphous counterpart in stabilizing the Pt catalysts. The enhanced electrochemical stability resulted from the addition of SnO₂ was explained by the interaction between Pt and SnO₂. Crystalline SnO₂ also increased the electrochemical surface area of Pt catalysts, resulting in higher activity.

© 2013 Elsevier B.V. All rights reserved.

1. Introduction

Proton-exchange membrane fuel cells (PEMFC) are efficient and environmentally friendly energy conversion devices. Their applications in both stationary and automotive powers have drawn extensive attention all over the world. However, its high cost and low life time, especially the low electrochemical durability and low electrocatalytic activity of electrocatalysts toward the oxygen reduction reaction (ORR) at the cathode, impede the wide commercialization of PEMFC [1,2].

Currently, the state-of-art electrocatalysts in PEMFC are Pt nanoparticles supported on carbon black. A great deal of efforts has been devoted to increase the electrochemical durability of the Pt electrocatalysts. We have demonstrated that Pt nanowires can effectively improve the electrochemical durability compared to Pt nanoparticles [3]. In addition, Pt nanotubes exhibited higher electrochemical stability than Pt nanoparticles [4]. R.R. Adzic's group reported highly stable Pt modified with Au clusters [5] and Pt monolayer on PdAu nanoparticles electrocatalyst [6]. K.C. Neyerlin reported that the dealloyed Pt–transition metal alloy catalysts showed higher stability than the commercial Pt/C catalyst [7].

In addition, support materials also have a significant impact on the electrochemical stability. Pt catalysts supported on high graphitic carbon exhibit higher durability than the low graphitic carbon [8,9]. Pt deposited on carbon nanotubes (Pt/CNT) shows higher stability and activity than Pt deposited on carbon black (Pt/C) [10,11]. Previously, we demonstrated that nitrogen-doped

* Corresponding author. Tel.: +1 519 661 2111x87759; fax: +1 519 661 3020.
E-mail address: xsun@eng.uwo.ca (X. Sun).

carbon nanotubes (CN_x) as supports can effectively improve the electrochemical stability [12] and electrocatalytic activity [13] of the supported Pt catalysts.

In this report, CN_x serve as a scaffold, upon which SnO_2 is controllably deposited and Pt is deposited subsequently to construct a Pt–SnO_2/CN_x hybrid electrocatalyst. Coincidentally, this electrocatalyst consists of a similar idea to a recent publication on Pt–ITO–graphene [14]. The electrochemical stability of the obtained hybrid electrocatalysts was investigated as the cathode catalysts in a PEMFC.

2. Experimental

2.1. Materials

Ferrocene (98%, Aldrich), melamine (99+%, Aldrich), tin(IV) chloride (99% $SnCl_4$, Sigma–Aldrich), $H_2PtCl_6\cdot6H_2O$ (ACS reagent, Sigma–Aldrich), ethylene glycol (anhydrous, 99.8%, Sigma–Aldrich), sodium borohydride ($\geq$99%, Fluka), 2-propanol (anhydrous, 99.5%, Sigma–Aldrich), H_2SO_4 (ACS reagent, 95.0–98.0%, Sigma–Aldrich).

2.2. Synthesis of CN_x

CN_x were synthesized via the floating catalyst chemical vapor deposition (FCCVD) method in a horizontal quartz tube furnace system (Lindburg/Blue), as described before in details [15]. A piece of carbon paper (E-TEK Division, PEMEAS Fuel Cell Technologies, Somerset, NJ) sputtered with a 30 nm Al buffer layer was applied as the substrate. 100 mg ferrocene and 2 g melamine were used as the catalyst and nitrogen precursor, respectively. CN_x were synthesized by the decomposition of ferrocene and melamine under a gas flow of Ar (500 sccm (standard cubic centimeters per minute), ultra high purity, Praxair) and ethylene (10 sccm) at 950 °C.

2.3. SnO_2 deposition

SnO_2 was deposited on the CN_x (SnO_2/CN_x) by atomic layer deposition (ALD) in a commercial ALD reactor (Savannah 100, Cambridge Nanotechnology Inc., USA) [16]. $SnCl_4$ and deionized water as precursors were introduced into the reactor in an alternating manner. Nitrogen (20 sccm) was applied as the carrier gas, and reactor was kept at the pressure of 0.4 Torr. The reaction was set for 50 cycles at 200 °C or 400 °C. The obtained materials are denoted as $SnO_2(200)$/CN_x and $SnO_2(400)$/CN_x, respectively.

2.4. Pt deposition

Pt nanoparticles were deposited on the obtained CN_x (or SnO_2/CN_x) with well-established ethylene glycol reduction method, as we reported before [13]. Ethylene glycol (100 mL) containing $H_2PtCl_6\cdot6H_2O$ and CN_x (or SnO_2/CN_x) at a Pt loading of 30 wt.% was refluxed at 160 °C for 3 h, and then cooled down to room temperature. The suspension was filtered and dried in a vacuum oven at 60 °C over night. Reacted with sodium borohydride, no changes happened to the colorless and transparent filtrate. This indicates that all H_2PtCl_6 was reduced and deposited on CN_x (or SnO_2/CN_x), and thus the same Pt loadings (30 wt.%) were obtained on the prepared catalysts. Inductively coupled plasma-optical emission spectroscopy (ICP-OES) also indicated a Pt loading close to 30 wt%. The obtained hybrid catalysts are denoted as Pt/CN_x, Pt–$SnO_2(200)$/CN_x and Pt–$SnO_2(400)$/CN_x, respectively.

2.5. Physical characterizations

The morphology of CN_x was characterized with field emission scanning electron microscopy (SEM, Hitachi S-4800, 5 kV).

Transmission electron microscopy (TEM, Philips CM10, 80 kV) was applied to characterize the structures of CN_x and the dispersions of Pt nanoparticles. High resolution TEM and energy dispersive X-ray spectra (EDS) were carried out on a JEOL 2010F at 200 kV to inspect the fine nanostructure of the catalysts and the relative elements.

2.6. Electrochemical characterizations

The electrochemical characterizations were conducted in a thermostatic standard three-compartment electrochemical cell using a ring-disk electrode setup with a bi-potentiostat (Model PGSTAT-30, Ecochemie, Brinkman Instruments) and rotation control (Pine Instruments). Pt wire and Ag/AgCl (3 M NaCl, CH Instruments, Inc.) served as the counter and reference electrode, respectively. For convenience, all potentials in this paper are referenced to standard hydrogen electrode (SHE).

The electrochemical stability was investigated with accelerated durability test (ADT) method [12]. A glassy carbon electrode (5 mm in diameter, Pine Instruments) casted with a thin film of the same amount catalysts was applied as the working electrode. 5 mg catalyst (Pt/CN_x, Pt–$SnO_2(400)$/CN_x or Pt–$SnO_2(200)$/CN_x) was suspended in 1 mL 2-propanol containing 20 μL of a 5 wt.% Nafion solution (Ion Power Inc., USA) with ultrasonication to achieve a uniform ink. The catalyst thin film was prepared by casting 20 μL of the ink onto a glassy carbon electrode (5 mm in diameter, Pine Instruments). The electrode was dried at 60 °C for 10 min. The electrode was first activated by potential cycling for about 30 cycles in N_2 saturated 0.5 M H_2SO_4 between 0.02 and 1.2 V. The electrochemical stability was evaluated with the accelerated durability test (ADT) method [12]. The electrode was cycled between 0.6 and 1.2 V for 4000 cycles in O_2 (ultra high purity, Praxair) saturated 0.5 M H_2SO_4 solution. Meanwhile, full-scale voltammograms (0.02–1.2 V) in N_2 (ultra high purity, Praxair) saturated 0.5 M H_2SO_4 solution were recorded before and post the ADT to track the degradation of Pt catalysts. The scan rate was kept at 50 mV s^{-1} constantly.

The catalytic activity for the ORR was evaluated with rotating ring-disk electrode (RRDE, 5 mm in diameter, Pine Instruments) in 0.5 M H_2SO_4 solution [13]. O_2 was bubbled for 30 min to achieve saturation. With gentle O_2 bubbling, RRDE tests were conducted at 5 mV s^{-1} by a negative scan with a rotation speed of 1600 rpm (revolution per minute). All the electrochemical experiments were carried out at 25 °C.

The electrode was activated by potential cycling for about 30 cycles in N_2 saturated 0.5 M H_2SO_4 between 0.02 and 1.2 V. CO (ultra high purity, Praxair) was then purged closed to the working electrode for 30 min with the electrode polarized at 0.2 V. The electrode was then purged with N_2 for 30 min under potential control to expulse the CO dissolved in the solution. The CO stripping voltammetry was conducted with a positive scan at 1 mV s^{-1}. The current was corrected based on the background current in N_2 saturated 0.5 M H_2SO_4 solution.

3. Results and discussion

Fig. 1 presents the SEM and TEM observations of the CN_x synthesized on carbon paper substrate. The carbon paper is totally covered with CN_x with high density according to the SEM image (Fig. 1a). The TEM image (Fig. 1b) shows the structural information of CN_x. Different from the tubular structure of general CNT, CN_x exhibit a bamboo-like structure with irregular interlinks along the tube, which is typical for the nitrogen doping. The diameters of CN_x range from 120 to 200 nm.

SnO_2 was deposited on the surface of CN_x with atomic layer deposition method at 200 and 400 °C. Applied as catalyst supports for PEMFCs, CN_x, $SnO_2(200)$/CN_x and $SnO_2(400)$/CN_x were
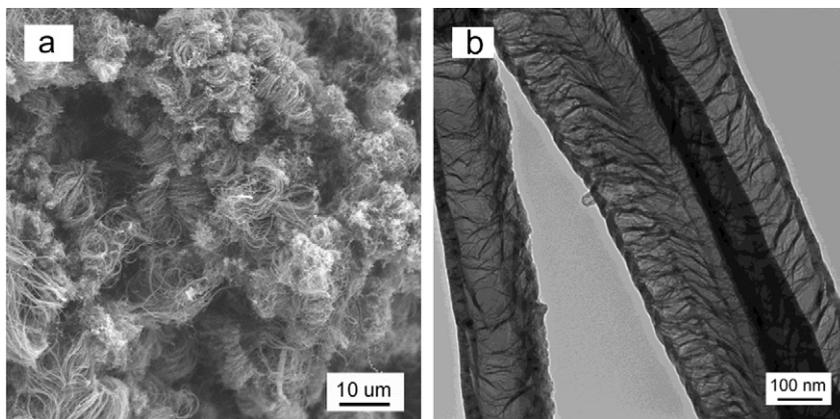
Fig. 1. SEM (a) and TEM (b) images of CN_x synthesized on carbon paper.

deposited with Pt nanoparticles with ethylene glycol reduction method. Fig. 2 exhibits the energy dispersive X-ray spectra (EDS) of Pt/CN_x, $Pt–SnO_2(200)/CN_x$ and $Pt–SnO_2(400)/CN_x$. The Cu signal in the three spectra is ascribed to the Cu grids of the sample holder. The strong Pt signals in the three spectra indicate that Pt has been successfully deposited on the supports. Compared to Pt/CN_x (Fig. 2a), $Pt–SnO_2(200)/CN_x$ (Fig. 2b) and $Pt–SnO_2(400)/CN_x$ (Fig. 2c) exhibit an extra Sn peak, which confirms the pre-deposited SnO_2.

The distributions of the Pt nanoparticles on the three supports are presented in Fig. 3a–c. In the three cases, Pt nanoparticles disperse uniformly on the support with similar sizes around 4 nm. This indicates that the pre-deposited SnO_2 does not have a remarkable influence on the distribution of the Pt nanoparticles. High resolution TEM (HRTEM) images provide more intuitive

Fig. 2. Energy dispersive X-ray spectra of (a) Pt/CN_x, (b) $Pt–SnO_2(200)/CN_x$ and (c) $Pt–SnO_2(400)/CN_x$.

information on the crystal structures of the three catalysts. Pt/CN_x (Fig. 3d), $Pt–SnO_2(200)/CN_x$ (Fig. 3e) and $Pt–SnO_2(400)/CN_x$ (Fig. 3f) all exhibit the features of CN_x supports and nanoparticles with a lattice spacing of 0.223 nm, which is ascribed to Pt (111) plane. The featureless gray nanoparticles on $Pt–SnO_2(200)/CN_x$ (Fig. 3e) are ascribed to amorphous SnO_2. Nanoparticles with a lattice spacing of 0.335 nm were observed on $Pt–SnO_2(400)/CN_x$ (Fig. 3f), which corresponds to SnO_2 (110) plane. This observation agrees well with our previous report that amorphous and polycrystalline SnO_2 can be selectively deposited at 200 and 400 °C, respectively [16]. Selected area electron diffraction (SAED) patterns (Fig. 3g–i) of the three catalysts all exhibit C (002), Pt (111), Pt (200) and Pt (311) crystal planes, which come from the CN_x support and Pt nanoparticles. Furthermore, diffraction patterns of SnO_2 (111) and SnO_2 (112) planes can be indexed from the $Pt–SnO_2(400)/CN_x$ pattern (Fig. 3i); while no SnO_2 information can be reflected from the SAED patterns on $Pt–SnO_2(200)/CN_x$ (Fig. 3h), implying amorphous nature of the SnO_2 on the $Pt–SnO_2(200)/CN_x$ sample, which is consistent with the HRTEM observations above.

Since the durability of the electrocatalyst is a big concern for the real application of fuel cells, accelerated durability test (ADT) [12] is employed to investigate the electrochemical durability of the three catalysts. It can be observed that the H_2 adsorption/desorption regions of the three electrocatalysts are suppressed in cyclic voltammograms (Figs. S1a, S2a and S3a in Supplementary data) and the linear scanning voltammograms for ORR shift negatively (Figs. S1b, S2b and S3b in Supplementary data) after the ADT. Both results suggest that the electrochemical surface area (ECSA) of the catalysts decreases and the electrocatalytic activities toward ORR decline after the ADT. That is, all three electrocatalysts degraded during voltammetric cycling of ADT. The double layer region in the cyclic voltammogram becomes thinner after the ADT tests, which was observed in our previous report about the durability of CN_x as the supports [12]. In cases of the catalysts with SnO_2 (Figs. S2 and S3 in Supplementary data) in this work, the changes of the double layer region after ADT are more obvious than the one without SnO_2 (Fig. S1 in Supplementary data). This can be attributed to the SnO_2 changes during ADT. Both the peaks around 0.7 V at the positive scan and 0.5 V at the negative scan are assigned to SnO_2 [23]. After the ADT tests, the two peaks become less obvious. The durabilities of the three catalysts are compared quantitatively by comparing the ECSA calculated from the H_2 adsorption/desorption charges [17] in cyclic voltammograms (Fig. 4a) and ORR currents at 0.85 V (Fig. 4b) before and after the ADT. As shown in Fig. 4a, only 39.9% of the initial ECSA remains on Pt/CN_x after ADT, which agrees well with our previous report [12]. $Pt–SnO_2(200)/CN_x$ and $Pt–SnO_2(400)/CN_x$
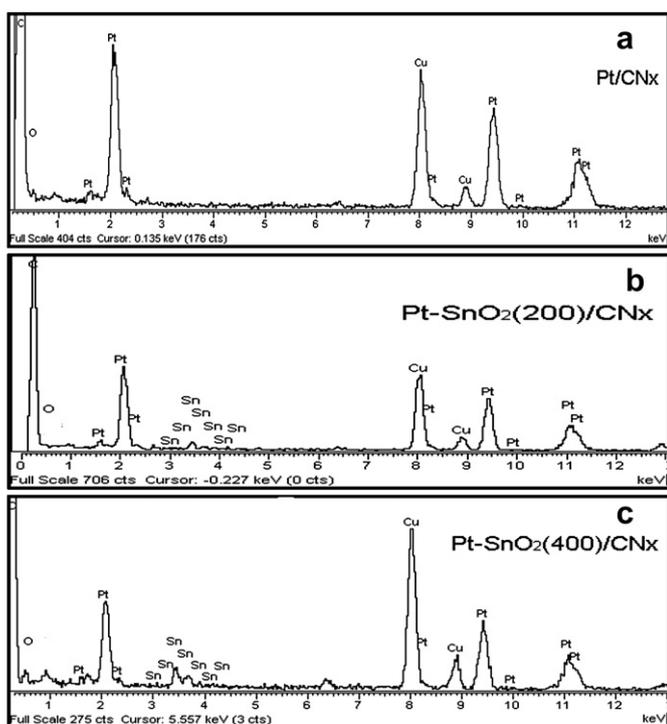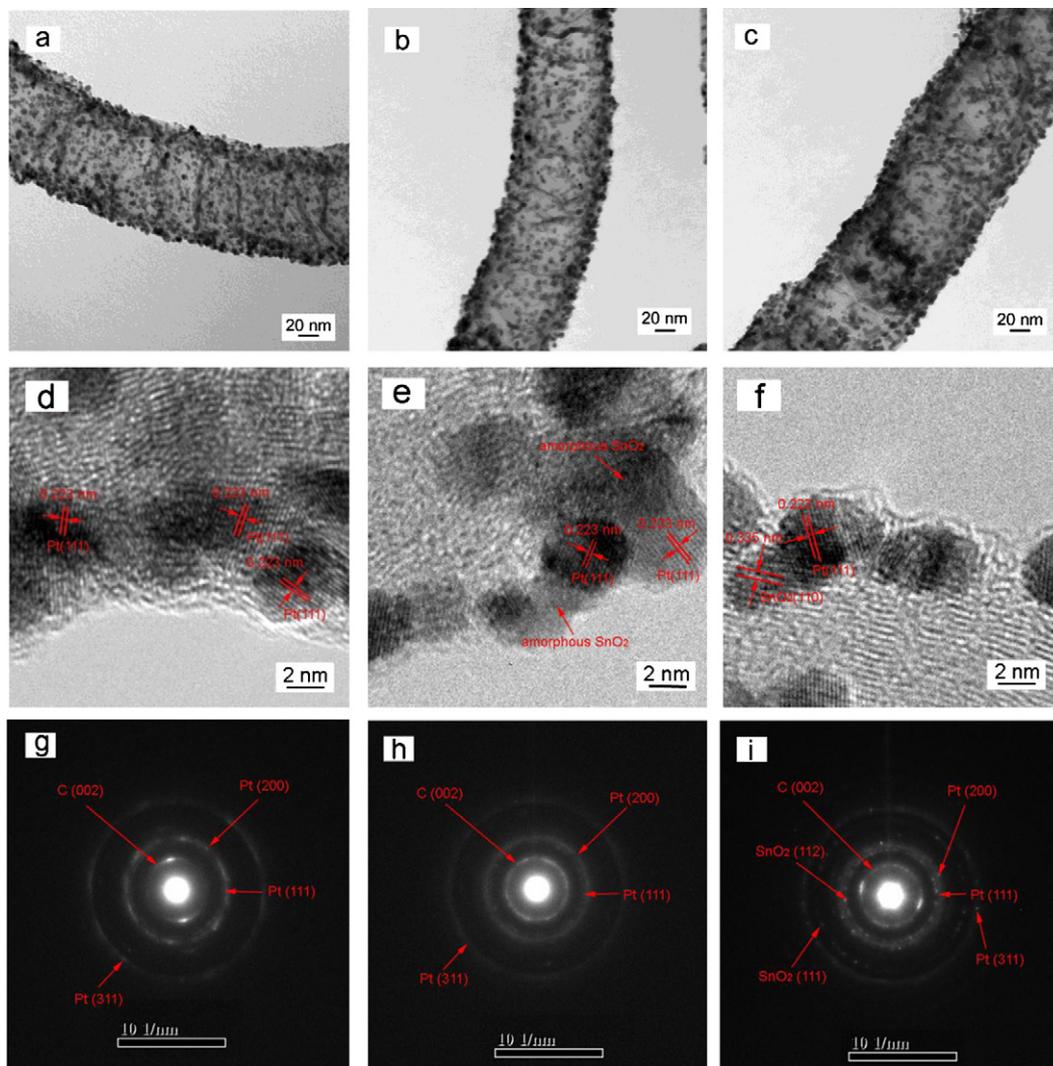
Fig. 3. The dispersion of Pt nanoparticles, high resolution transmission electron microscopy and selected area electron diffraction patterns of (a, d, g) Pt/CN$_x$, (b, e, h) Pt–SnO$_2$(200)/CN$_x$ and (c, f, i) Pt–SnO$_2$(400)/CN$_x$.

keep 53.7% and 62.1% of the initial ECSA, respectively. 35.3, 45.5 and 57.4% of the initial ORR current at 0.85 V remains on Pt/CN$_x$, SnO$_2$(200)/CN$_x$ and Pt–SnO$_2$(400)/CN$_x$, respectively, as presented in Fig. 4b. These results manifest that SnO$_2$ can effectively enhance the electrochemical durability of Pt catalyst, and crystalline SnO$_2$ is more effective than amorphous SnO$_2$ in stabilizing Pt catalysts.

The higher electrochemical stability with SnO$_2$ can be attributed to the strong interaction between the Pt and SnO$_2$. It has been reported that metal oxides can anchor Pt nanoparticles by interacting with Pt and thereby inhibit the migration and agglomeration of Pt [18]. The improved durability has also been obtained with TiO$_2$, [19,20], Ti$_{0.7}$W$_{0.3}$O$_2$, [21] and CeO$_x$ [22]. Pt electrocatalysts supported on carbon-free SnO$_2$ [23] and Sb-doped SnO$_2$ [24] also
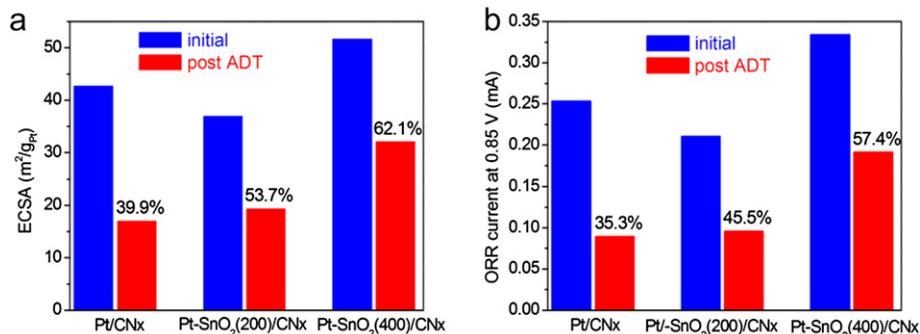

Fig. 4. The comparisons of (a) the ECSA and (b) ORR current at 0.85 V of Pt/CN$_x$, Pt–SnO$_2$(200)/CN$_x$ and Pt–SnO$_2$(400)/CN$_x$ before and after ADT.

demonstrated higher electrochemical stability than Pt/C. The strong interaction between Pt and SnO_2 is confirmed by the CO stripping behaviors of the three catalysts, as presented in Fig. 5. Pt/CN_x shows a single sharp peak centered at 0.762 V. Whereas, the CO electrochemical oxidation peak on both $Pt–SnO_2(200)/CN_x$ and $Pt–SnO_2(400)/CN_x$ split into two broad peaks, with a strong peak at 0.624 V and a weak shoulder peak at 0.728 V. The major oxidation peak potential of the absorbed CO shifts 138 mV negatively with SnO_2. The removal of CO absorbed on Pt surface requires OH groups from either the Pt surface at a high potential or SnO_2 surface at a low potential. It is worth to be noted that the diffusion of OH group on metal oxide surface is slow [25]. Therefore, the promotional removal of CO by SnO_2 needs a close interaction between Pt and SnO_2. This large negative shift in CO stripping peak indicates a strong interaction between Pt and SnO_2. The HRTEM images in Fig. 3e and f also provide direct evidence that Pt and SnO_2 interact closely. As discussed above, $Pt–SnO_2(400)/CN_x$ has a higher durability than $Pt–SnO_2(200)/CN_x$. Since the same procedure was adopted, the only difference between $Pt–SnO_2(400)/CN_x$ and $Pt–SnO_2(200)/CN_x$ is that SnO_2 in $Pt–SnO_2(400)/CN_x$ is crystalline, while SnO_2 in $Pt–SnO_2(200)/CN_x$ is amorphous. Therefore, the higher electrochemical stability of $Pt–SnO_2(400)/CN_x$ than $Pt–SnO_2(200)/CN_x$ can be attributed to the structural difference of SnO_2 nanoparticles. Take a review at the CO stripping (Fig. 5), the ratio between the strong peak at low potential and the weak peak at high potential of $Pt–SnO_2(400)/CN_x$ and $Pt–SnO_2(200)/CN_x$ is 2.2 and 1.6, respectively. CO is more easily oxidized with crystalline SnO_2 than the amorphous counterpart. This implies that there is a stronger interaction between Pt and crystalline SnO_2 than amorphous SnO_2. The stronger interaction results in a higher electrochemical stability of $Pt–SnO_2(400)/CN_x$ than that $Pt–SnO_2(200)/CN_x$.

Despite of the similar Pt sizes of the three catalysts shown in Fig. 3a–c, the initial ECSA of the three catalysts are different. The initial ECSA of Pt/CN_x, $Pt–SnO_2(200)/CN_x$ and $Pt–SnO_2(400)/CN_x$ are 42.67, 36.91 and 51.63 $m^2\ g_{Pt}^{-1}$ from the H_2 adsorption/desorption regions in Figs. S1a, S2a and S3a in Supplementary data. CO stripping curves are also adopted to calculate the ECSA, which are 41.48, 38.02, 53.21 $m^2\ g_{Pt}^{-1}$ for Pt/CN_x, $Pt–SnO_2(200)/CN_x$ and $Pt–SnO_2(400)/CN_x$. The two sets of values for ECSA are close to each other. The positive effect of crystalline SnO_2 on the ECSA of Pt is in line with other reports [26,27]. This can be
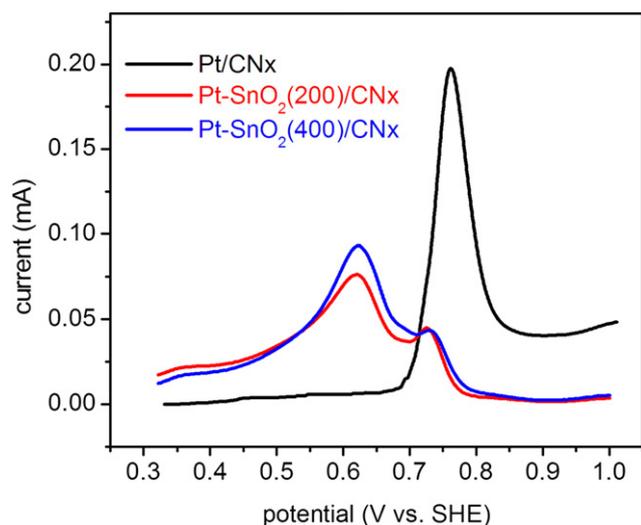
explained by the lateral effect of oxygenate species on SnO_2. The lateral repulsion from the oxygenate species on the SnO_2 surface inhibits the generation of oxygen species on the adjacent Pt and so keeps a clean metallic surface. The low electrical conductivity of amorphous SnO_2 in $Pt–SnO_2(200)/CN_x$ may electrically block some of the Pt nanoparticles deposited subsequently and results in a smaller ECSA.

4. Conclusions

In summary, this work demonstrates that the electrochemical durability of Pt can be enhanced by SnO_2 as the co-catalyst. The structure of SnO_2 has a remarkable influence on the stability of Pt catalyst. Crystalline SnO_2 is more effective than the amorphous one to improve the stability of Pt catalyst. The crystalline SnO_2 can also increase the electrochemical surface area of Pt catalyst. The present report provides guidance on searching for Pt catalysts to achieve both high activity and durability, and will benefit the commercialization of PEMFCs.

Appendix A. Supplementary data

Supplementary data associated with this article can be found in the online version, at http://dx.doi.org/10.1016/j.jpowsour.2013.03.093.

References

[1] R. Borup, J. Meyers, B. Pivovar, Y.S. Kim, R. Mukundan, N. Garland, D. Myers, M. Wilson, F. Garzon, D. Wood, P. Zelenay, K. More, K. Stroh, T. Zawodzinski, J. Boncella, J.E. McGrath, M. Inaba, K. Miyatake, M. Hori, K. Ota, Z. Ogumi, S. Miyata, A. Nishikata, Z. Siroma, Y. Uchimoto, K. Yasuda, K.-i. Kimijima, N. Iwashita, Chem. Rev. 107 (2007) 3904–3951.
[2] Y. Shao, G. Yin, Y. Gao, J. Power Sources 171 (2007) 558–566.
[3] S. Sun, G. Zhang, D. Geng, Y. Chen, R. Li, M. Cai, X. Sun, Angew. Chem., Int. Ed. 50 (2011) 422–426.
[4] Z. Chen, M. Waje, W. Li, Y. Yan, Angew. Chem., Int. Ed. 46 (2007) 4060–4063.
[5] J. Zhang, K. Sasaki, E. Sutter, R.R. Adzic, Science 315 (2007) 220–222.
[6] K. Sasaki, H. Naohara, Y. Choi, Y. Cai, W. Chen, P. Liu, R.R. Adzic, Nat. Commun. 3 (2012) 1115.
[7] K.C. Neyerlin, R. Srivastava, C. Yu, P. Strasser, J. Power Sources 186 (2009) 261–267.
[8] Y. Shao, S. Zhang, R. Kou, X. Wang, C. Wang, S. Dai, V. Viswanathan, J. Liu, Y. Wang, Y. Lin, J. Power Sources 195 (2010) 1805–1811.
[9] P.V. Shanahan, L. Xu, C. Liang, M. Waje, S. Dai, Y.S. Yan, J. Power Sources 185 (2008) 423–427.
[10] X. Wang, W. Li, Z. Chen, M. Waje, Y. Yan, J. Power Sources 158 (2006) 154–159.
[11] Y. Shao, G. Yin, Y. Gao, P. Shi, J. Electrochem. Soc. 153 (2006) A1093–A1097.
[12] Y. Chen, J. Wang, H. Liu, R. Li, X. Sun, S. Ye, S. Knights, Electrochem. Commun. 11 (2009) 2071–2076.
[13] Y. Chen, J. Wang, H. Liu, M.N. Banis, R. Li, X. Sun, T.K. Sham, S. Ye, S. Knights, J. Phys. Chem. C 115 (2011) 3769–3776.
[14] R. Kou, Y. Shao, D. Mei, Z. Nie, D. Wang, C. Wang, V.V. Viswanathan, S. Park, I.A. Aksay, Y. Lin, Y. Wang, J. Liu, J. Am. Chem. Soc. 133 (2011) 2541–2547.
[15] H. Liu, Y. Zhang, R. Li, X. Sun, S. Desilets, H. Abou-Rachid, M. Jaidann, L.-S. Lussier, Carbon 48 (2009) 1498–1507.
[16] X. Meng, Y. Zhong, Y. Sun, M.N. Banis, R. Li, X. Sun, Carbon 49 (2011) 1133–1144.
[17] M.S. Saha, R. Li, X. Sun, J. Power Sources 177 (2008) 314–322.
[18] C.C. Shih, J.R. Chang, J. Catal. 240 (2006) 137–150.
[19] S.Y. Huang, P. Ganesan, S. Park, B.N. Popov, J. Am. Chem. Soc. 131 (2009) 13898–13899.
[20] X. Liu, J. Chen, G. Liu, L. Zhang, H. Zhang, B. Yi, J. Power Sources 195 (2010) 4098–4103.

Fig. 5. Background corrected CO strippings on Pt/CN_x, $Pt–SnO_2(200)/CN_x$ and $Pt–SnO_2(400)/CN_x$ in 0.5 M H_2SO_4 at 1 mV s^{-1}.

[21] D. Wang, C.V. Subban, H. Wang, E. Rus, F.J. DiSalvo, H.D. Abruna, J. Am. Chem. Soc. 132 (2010) 10218–10220.
[22] K. Fugane, T. Mori, D.R. Ou, A. Suzuki, H. Yoshikawa, T. Masuda, K. Uosaki, Y. Yamashita, S. Ueda, K. Kobayashi, N. Okazaki, I. Matolinova, V. Matolin, Electrochim. Acta 56 (2011) 3874–3883.
[23] A. Masao, S. Noda, E. Takasaki, K. Ito, K. Sasaki, Electrochem. Solid-State Lett. 12 (2009) B119–B122.
[24] K.S. Lee, I.S. Park, Y.H. Cho, D.S. Jung, N. Jung, H.Y. Park, Y.E. Sung, J. Catal. 258 (2008) 143–152.
[25] H. Yuan, D. Guo, X. Li, L. Yuan, W. Zhu, L. Chen, X. Qiu, Fuel Cells 9 (2009) 121–127.
[26] L. Jiang, L. Colmenares, Z. Jusys, G.Q. Sun, R.J. Behm, Electrochim. Acta 53 (2007) 377–389.
[27] R.S. Hsu, D. Higgins, Z. Chen, Nanotechnology 21 (2010) 165705.